Structural, optical and magnetic properties of Cr doped ZnO microrods prepared by spray pyrolysis

S Yılmaz[1,4], M Parlak[2], Ş Özcan[3], M Altunbaş[1], E Bacaksiz[1] and E McGlynn[4]

[1] Department of Physics, Karadeniz Technical University, 61080 Trabzon, Turkey
[2] Department of Physics, Middle East Technical University, 06531 Ankara, Turkey
[3] SNTG Lab., Physics Engineering Department, Hacettepe University, Beytepe, 06800 Ankara, Turkey
[4] School of Physical Sciences, National Centre for Plasma Science and Technology, Dublin City University, Glasnevin, Dublin 9, Ireland

E-mail: s_yilmaz@ktu.edu.tr

Abstract

A series of Cr-doped ZnO micro-rod arrays were fabricated by a spray pyrolysis method. X-ray diffraction patterns of the samples showed that the undoped and Cr-doped ZnO microrods exhibit hexagonal crystal structure. Surface morphology analysis of the samples has revealed that pure ZnO sample has a hexagonal microrod morphology. From X-ray photoelectron spectroscopy studies, the Cr 2p3/2 binding energy is found to be 577.34 eV indicating that the electron binding energy of the Cr in ZnO is almost the same as the binding energy of Cr^{3+} states in Cr_2O_3. The optical band gap E_g decreases slightly from 3.26 to 3.15 eV with the increase of actual Cr content from x = 0.00 to 4.63 at % in ZnO. Photoluminescence studies at 10 K show that the incorporation of chromium leads to a relative increase of deep level band intensity. It was also observed that Cr doped samples clearly showed ferromagnetic behavior; however, 2.49 % Cr doped ZnO showed remnant magnetization higher than that of 1.07 % and 4.63 % Cr doped samples, while 4.63 % Cr doped ZnO samples had a coercive field higher than the other dopings.

1. Introduction

In recent years, much attention has been paid to Diluted Magnetic Semiconductors (DMSs) formed by the partial replacement of cations in a non-magnetic semiconductor by magnetic transition metal ions for spintronic applications. Spintronics as a field investigates the applications of carrier spin transport as well as charge transport in a new generation of devices such as spin-valve transistors [1], spin light-emitting diodes [2] and logic devices [3]. To realize these devices it is necessary to develop semiconducting materials that show ferromagnetic behavior at room temperature. Among the different types of wide-

Corresponding address: Department of Physics, Faculty of Sciences, Karadeniz Technical University, 61080, Trabzon, Turkey.

band-gap semiconductors ZnO, with a direct band gap of 3.37 eV and a large exciton binding energy of 60 meV, has become one of the most important functional semiconducting materials for electro-optical devices like UV light emitters [4], piezoelectric transducers [5] and gas sensors [6]. Doping ZnO with transition metals has received considerable interest due to its room temperature ferromagnetism [7-9]. In 2000, Dietl et al [10] predicted theoretically that Mn doped ZnO and GaN would be ferromagnetic at room temperature and would therefore be suitable for applications in spintronics. Following this initial work, using ab initio calculations based on the local density approximation, Sato et al. [11] theoretically demonstrated that V-, Fe-, Co-, Ni- and Cr-doped ZnO showed ferromagnetic ordering above the room temperature. However, the reported experimental results on the studies of Cr-doped ZnO have been very conflicting. Some studies reveal that the magnetic behavior of Cr-doped ZnO appears to be very sensitive to the deposition method. For example, Ueda et al. [7] did not observe any ferromagnetic behaviour for Cr-doped ZnO film grown by pulse laser deposition, whereas Roberts et al. [12] prepared Cr-doped ZnO via magnetron sputtering and obtained ferromagnetic ordering at a doping concentration of 9.5 at.%. Furthermore, the results of Jin et al. [13] showed no ferromagnetic behavior for Cr-doped ZnO film at low temperatures even down to 3 K. Lee et al. [14] did not find ferromagnetism in sol–gel synthesized $Zn_{1-x}Cr_xO$ thin films, however obvious ferromagnetism appeared when the same films were co-doped with Li. Although there are many experimental studies on magnetic and non-magnetic doped ZnO films showing room temperature ferromagnetism, there is no consensus on the origin of ferromagnetism ZnO-based materials [7,15,16]. Early studies explained that a free carrier mediated mechanism was responsible for the ferromagnetic behavior [17]. However, more recent studies proposed that defects like oxygen vacancies give rise to ferromagnetic ordering in oxide based DMS [18].

In summary, ZnO in thin film form can be deposited within a wide variety of chemical techniques with a low cost of equipment [19,20] and lead to good quality ZnO thin films doped with different transition metals. In this work, our interest is the incorporation of Cr as an active impurity in the ZnO lattice which is of interest to increase in the chemical stability and magnetic properties. We have deposited Cr-doped ZnO micro-rods on glass substrates by the spray pyrolysis method and the effects of

Cr doping on the structural, magnetic and optical properties of the deposited ZnO microrods were investigated.

2. Experimental procedure

$Zn_{1-x}Cr_xO$ micro-rod arrays with nominal molar fraction (x) values of 0.00, 0.02, 0.04 and 0.06 were prepared by spray pyrolysis method in an air atmosphere. The experimental setup and other experimental procedures are explained in more detail elsewhere [21]. The initial stock solution was prepared from zinc chloride ($ZnCl_2$) at 0.1 M concentration in deionized water. Doping was achieved by the addition of $CrCl_3.6H_2O$ (0.1 M) to the stock solution, which was then sprayed on the glass substrate. The growth was performed with a spray rate of about 5 ml/min and a growth rate of ~ 50 nm/min. Prior to growth, glass substrates were cleaned in ethanol and then dried in vacuum. During the growth, the substrates were rotated with a speed of 10 revolutions per minute and the substrate was held at a temperature of 550 °C. The average thickness of the samples measured by means of cross-sectional images of the samples using scanning electron microscopy (SEM) was found to be ~ 5 μm, in all cases. The X-ray diffraction (XRD) data of the samples in θ-2θ mode were taken using a Bruker AXS D8 advance texture diffractometer with CuK_α radiation over the range 2θ=20–60° at room temperature. The surface morphology and bulk composition were studied with a JEOL JST-6400 SEM equipped with EDS (Energy Dispersive X-ray Spectroscopy). An acceleration voltage of 20 kV was used in all cases for this study. The chemical composition and bonding types in the surface and near-surface regions of the deposits were examined by x-ray photoelectron spectroscopy (XPS) using an UNISPECS ESCA system equipped with a Mg K_α x-ray radiation source of 1253.6 eV-energy. The kinetic energies of emitted electrons from the surface of the sample were analyzed by a concentric hemispherical analyzer, which operates in the constant pass-energy (CAE) mode, under high vacuum of about $1.3x10^{-7}$ Pa. The surface of the as-grown samples was sputtered by Ar ions before XPS in order to clean the surfaces and avoid contributions from unintentionally deposited C and O contamination due to atmospheric exposure. Due to charging effects, the C 1s photoelectron peak at 285.0 eV was consistently used as a reference for the charge-correction of binding energies of core levels and Auger peaks. Optical transmission measurements were performed at

room temperature with a Shimadzu UV-1201 UV–VIS–NIR spectrophotometer over a wavelength range of 300–1100 nm. Photoluminescence (PL) measurements were performed at both 10 K and 300 K, a SPEX 1704 monochromator, with a closed cycle cryostat Janis SHI-950-5. PL spectra were excited with the 325 nm line of a He–Cd laser at 22 mW. Magnetization measurements of the samples as a function of magnetic field and temperature were carried out using a Quantum Design Physical Property Measurement System (PPMS) system with a vibration sample magnetometer module.

3. Results and discussion

The structural properties of undoped ZnO and Cr-doped ZnO miro-rod arrays produced by the spray pyrolysis method were investigated by XRD, and the results for all samples are shown in figure 1(a)-(d). The XRD patterns of these samples are in good agreement with the JCPDS standard (No. 36-1451) data of wurtzite (hexagonal) ZnO powder. It was seen that undoped and Cr-doped ZnO samples exhibit peaks corresponding to (100), (002), (101) and (102) planes, with the (002) peak showing the highest intensity in all cases, implying that all the samples have a hexagonal crystal structure with a preferred orientation with the substrate normal parallel to the normal to the ZnO (002) plane. No peaks belonging to Cr metal, Cr oxides or other impurity phases were detected within the sensitivity of our XRD measurements, indicating that the dopant was incorporated into the host lattice. These data indicate that Cr doping does not substantially alter the deposited crystal structure and orientation. The calculated values for the c-axis lattice constant, based on the diffraction peak positions, were found to decrease from 5.21 Å for undoped to 5.19 Å for nominally 6 % Cr doped ZnO. The decrease in the lattice parameter *c* upon Cr incorporation indicates that the samples were in a state of strain and that along the c-axis this strain was compressive [22]. The reason for the change in this lattice parameter may be due to the concentration of foreign atoms and defects, and their difference of ionic radii with respect to the substituted matrix ion ions; since the radius of Cr^{3+} ions (0.63 Å) is smaller than that the Zn^{2+} ions (0.74 Å) and the Cr-O bond in Cr_2O_3 is shorter than the Zn-O bond in ZnO (1.96 Å compared to 1.98 Å) [23, 24] this is consistent both with the XRD data above and also with the XPS data below. The other possible reason for the change in lattice

constant may be due to the differences in the linear thermal expansion coefficients of ZnO samples with different Cr molar fractions and soda-lime glass [25].

Chemical compositions of undoped and Cr doped ZnO microrods were investigated by energy dispersive X-ray spectroscopy (EDS). Table 1 indicates that all the samples are composed of Zn, O or Cr, demonstrating that the existence of chromium within the samples as well as the increase in concentration of Cr in ZnO microrods. Table 1 also implies that actual atomic percentage ratio of Cr is less than the nominal composition in the solution. The difference between the actual and the nominal Cr concentration is probably due to the dilution of Cr ions in the ZnO host matrix. In addition, compared to undoped ZnO, it was found that the Cr doped ZnO microrods were zinc deficient and oxygen rich, indicating that the Cr doped ZnO samples were non-stoichiometric, beyond that expected for Zn replacement by Cr. Similar results were obtained by Wang et al. [26] for Cu doped ZnO nanoparticle sheets.

SEM surface micrographs for the samples are shown in figure 2 and reveal that undoped, 1.07, 2.49 and 4.63 % Cr-doped samples have hexagonal shaped microrods with sub-micron diameters. Compared to the undoped ZnO, it was observed that the morphology of the microrods exhibits no essential difference with the increase of Cr doping. However, there is some variation in microrod diameter within individual samples and between undoped samples and samples with different levels of Cr doping as illustrated in figure 2. Consistent with the XRD data in figure 1, the hexagonal microrods were seen to be aligned with their long axis (the c-axis based on the rods hexagonal cross-sectional shape) almost perpendicular to the substrate, indicating that rods preferentially grow with their long axis along the [002] crystallographic direction (c-axis) and that this direction is aligned normal to the glass substrate.

The chemical nature of the surface of undoped and Cr-doped ZnO rod was investigated in detail by XPS measurements. Figure 3 shows the XPS survey spectrum of undoped and 4.63 % Cr-doped ZnO microrods. Comparing our data with tabulated binding energy values, the survey spectrum indicates the presence of Zn, Cr, C and O elements on the surface and near surface region of the samples as assigned in figure 3. XPS measurements for undoped ZnO show that the main features located at 1022.00 and 1045.28 eV can be assigned to Zn 2p3/2 and Zn 2p1/2, respectively. These peaks shifted to slightly lower binding energy for 4.63 at.% Cr-doped ZnO as revealed in table 2. The inset of figure 3 shows the Cr 2p

spectrum for 4.63 at.% Cr-doped ZnO. As can be seen from the inset, the 2p level is split into a doublet with an energy separation due to the spin–orbit interaction [27]. As shown in table 2, the Cr 2p3/2 and 2p1/2 binding energies are 577.34 and 586.22 eV corresponding to Cr^{3+} 2p3/2 which are different from that of Cr metal (574.0 eV) and 576.3 eV of Cr^{4+} for pure CrO_2 which match well with the reported binding energy 577.0–577.2 eV of the 2p3/2 level of Cr^{3+} states [28-31]. It suggests that Cr dopants are indeed incorporated into the ZnO lattice, on Zn sites, as Cr^{3+} ions instead of Cr^{2+} ions [32,33].

The optical transmission spectra at room temperature of the undoped and Cr-doped ZnO microrod arrays are shown in figure 4. The transmittance spectra revealed that all samples had a low average transmittance at photon energies below the band gap. The maximum transmission of the undoped ZnO microrods was around 20 %. Depending on Cr content in the structure, transmission values increase from 20 % to 50 % as increasing the content from x = 0.00 to 4.63 at %. It is worth notifying that the low sub-bandgap transmission may well be due to scattering effects caused by the microrod microstructure of the deposit, which presents a very non-planar surface. Films having smoother surface morphology generally show higher transmittance [34]. Figure 4 also indicates that the absorption edge shifted slightly to higher wavelengths as the concentration of Cr increases in the ZnO microrods.

In order to determine the optical band gap energy, E_g, from the absorption spectra we used a Tauc-plot analysis of the variation of the absorption coefficient (α) with photon energy, with the relation;

$$\alpha(h\nu) = A(h\nu - E_g)^{1/2} \qquad (1)$$

where E_g is the optical band gap of the samples and A is a constant. Figure 5 shows the plots of $(\alpha h\nu)^2$ versus ($h\nu$) for the various ZnO microrod array samples. Extrapolations of the linear portions of the plots onto the energy axis were used to estimate the band gap values using this method and these analyses show an apparent decrease in E_g decreases from 3.26 to 3.15 eV with an increase of Cr content from x = 0.00 to 4.63 at %. This result is in agreement with the results reported on Cr doped ZnO film prepared by other techniques showing a slight red shift in the band gap [35]. However, an opposite trend (a band gap increase) with increasing Cr content in ZnO samples was also predicted in the literature [36]. We comment further below on the reliability of these band gap estimations.

Figure 6 shows low temperature PL spectra measured at 10 K of undoped and Cr-doped ZnO microrods. The UV peaks of all the samples are located at 3.361 eV and are ascribed to the near band edge (NBE) emission of excitons bound to donors (D^0X, members of the so-called I lines) [37]. The energies of these peaks are identical within about 2 meV for all samples, indicating that the dominant donor bound exciton emission energy is unaffected by the Cr incorporation. This D^0X emission is observed at a constant energy below the bandgap and thus indicates that the band gaps at low temperatures in all samples are identical, and hence these data are in clear disagreement with the variations in the band gap value determined by the Tauc plots presented above. The low temperature PL data give a very precise value for the band gap due to the sharp emission lines and these data provide clear evidence that the band gaps of all samples are unchanged by Cr incorporation. The origin of this disagreement is easily explained. The Tauc relation in equation (1) above assumes free carrier behaviour with no electron-hole interactions, whereas for ZnO the large excitonic binding energy of 60 meV means that significant electron-hole correlation is present even at room temperature and the so-called Sommerfeld enhancement factor is clearly seen in absorption spectra at room temperature [38-40]. Thus the use of the Tauc plot analysis is inappropriate for materials such as ZnO, unless correction is made for such excitonic effects. Changes in the absorption edge shape in figure 4, to which the Tauc analysis above is very sensitive, may actually indicate a change in the Sommerfeld factor in absorption due to changes in excitonic stability and consequently its spectral bandwidth, rather than a change in band gap. For these reasons we judge the conclusion from the low temperature PL data above, i.e. that the band gaps of the samples are unaffected by Cr doping, to be the correct one.

The undoped ZnO sample also exhibits three peaks located at 3.287 eV, 3.219 eV and 3.146 eV, respectively, in the band edge region. These peaks correspond closely to the first three longitudinal-optical (LO) phonon replicas of the D^0X emission, with a spacing close to the LO phonon energy of ~ 72 meV [41]. After doping the ZnO microrods with Cr, these peaks reduce dramatically, due to a reduction in the relative intensity of the near band edge emission, as shown in figure 6. In the deep level visible emission region, the Cr doped samples display a broad defect-related visible luminescence band which

increased in relative intensity, compared to the UV peak, with increased Cr doping level. The PL data thus shows evidence for an increase in optically active deep level defects with increased Cr doping level.

In order to understand the magnetic behavior of the microrods, the magnetization versus the field dependence curves of the samples corresponding to the actual compositions x = 1.07, 2.49 and 4.63 at % were measured at 300 K and are shown in figure 7. The diamagnetic contribution from the substrate is subtracted from the total magnetization. All three loops are found to be hysteretic, indicating ferromagnetic behavior at room temperature. The 1.07, 2.49 and 4.63 % Cr-doped samples possess the remnant magnetizations of ~ 1.56, ~ 4.86, and ~ 1.97 emu/cm^3, respectively, and their coercive forces (H_c) are ~ 251, ~ 168 and ~ 348 Oe, respectively. It is clear that all three samples showed clear ferromagnetic behavior, however, the 2.49 % Cr-doped ZnO sample showed a remnant magnetization higher than that of 1.07 % and 4.63 % Cr doped samples, while the 4.63 % Cr-doped sample showed the highest coercive field.

In principle, as the Cr concentration in ZnO samples increases, a number of antiferromagnetic phases may occur such as Cr metal, Cr_2O_3 and Cr_3O_4 [42]. However these phases will not contribute to ferromagnetism, except in the case of the CrO_2 phase [43]. These phases weren't observed in our samples by XRD measurements. Therefore, based on the discussion above, room temperature ferromagnetism in our Cr-doped ZnO sample is from the ferromagnetic interaction between the Cr ions substituting for Zn lattice ions rather than from the chromium oxide inclusions.

Several groups have found that the intrinsic defects play crucial roles in the ferromagnetism of Cr doped ZnO. For example, Liu et al. [44] indicated that point defects such as Zn_i or V_{Zn} are responsible for ferromagnetism in Cr:ZnO and Hong et al. [45] have pointed out that the magnetization in their Cr:ZnO films is related to oxygen vacancies (V_o). Li et al. [46] also investigated the magnetic properties of Cr-doped ZnO samples prepared under a high magnetic field. Samples prepared under a 4 T field showed clear ferromagnetic behavior at room temperature, whereas other samples prepared without magnetic field showed no ferromagnetic behavior, possibly indicating that the interaction between Zn vacancies and Cr dopants contributes to the origin of ferromagnetism in Cr-doped ZnO. Furthermore, Liu et al. [47] suggested that two key factors lead to the appearance of ferromagnetism in transition metal(TM)-doped

ZnO nanocrystals: one is the increase of the number of defects and oxygen vacancies, the other is the exchange interactions between the TM ions and the O ion spin moment. Similarly, Chu et al. [48] reported theoretical calculations showing that the origin of magnetic properties of Cr:ZnO films is induced by Cr 3d and O 2p spin moments.

With regard to the origin of the ferromagnetism observed in our samples and considering the full range of XRD, XPS and optical measurements, our data would support the hypothesis that the magnetic behavior observed is related to the presence of intrinsic defects. As discussed previously, PL spectra can provide information on optically active deep level defects in the Cr doped ZnO microrods. From figure 6, the relative intensity of the deep level band for Cr doped ZnO samples is larger than that of undoped ZnO, indicating that Cr doping may increase the concentration of defects such as oxygen vacancies and Zn interstitial, consistent with the hypothesis that such defects may be the origin of the room temperature ferromagnetism observed in our samples [49,50]. Defect complexes such as V_{Zn} + Cr_{Zn} and V_O + Cr_{Zn} may also form during the deposition Cr-doped ZnO microrods and may contribute to the ferromagnetic behavior [51]. Electrons trapped locally by these defects may occupy an orbital overlapping with the *d* shell of TM neighbors to form bound magnetic polarons [52].

Magnetization versus temperature (M–T) curves was also measured in the temperature range of 5-300 K and is plotted in figure 8. As seen from this figure, the temperature dependence of the magnetization of the 2.49 at % Cr-doped ZnO sample is linear at high temperatures. At lower temperatures it displays a steep rise with pronounced concave curvature but without showing any distinct magnetic phase transition. Based on these data we can conclude that the Curie temperature for this sample is well above room temperature, but it is hard to determine the exact value, since the value of the Curie temperature is rather high, exceeding the range of our measurements. Quite a number of works in the literature have shown that Cr-doped ZnO shows ferromagnetism at Curie temperatures above room temperature [47,53].

4. Conclusions

Based on the XRD, SEM, XPS, optical absorption, PL and magnetic measurements of our samples the following main points emerge: (i) the undoped sample had a hexagonal structure with a strong (002) preferred orientation. Cr incorporation did not significantly change the texture or the morphology but did lead to a slight reduction in c-axis lattice constant; (ii) XPS studies show that Cr doping alters the surface composition of the ZnO microrods and bonds with oxygen atoms in the structure. The Cr 2p3/2 and 2p1/2 binding energies are seen at 577.34 and 586.22 eV corresponding to Cr^{3+} indicating that the electron binding energy of Cr in ZnO is similar to that in pure Cr_2O_3; (iii) compared to the undoped ZnO, the number of optically active deep level defects increased for Cr doped ZnO microrod samples; (iv) magnetic measurements indicated that the Cr-doped ZnO samples show ferromagnetic behavior at room temperature.

These data allow us to further conclude that Cr in Cr doped ZnO microrods prepared by spray pyrolysis is incorporated in the lattice on Zn sites and as Cr^{3+} ions instead of Cr^{2+} ions, and that deep level intrinsic defects and complexes may be the origin of the room temperature ferromagnetism observed in these samples, consistent with other reports in the literature.

Acknowledgement: This work was supported by the research fund of Karadeniz Technical University, Trabzon, Turkey, under contract no. 2008.111.001.9. The corresponding author (SY) also gratefully acknowledges the support of the Council of Turkish Higher Education in the form of a fellowship to support extended visits to foreign institutions.

Figure Captions

Figure 1. XRD patterns of (a) undoped, (b) 1.07 % Cr-, (c) 2.49 % Cr and (d) 4.63 % Cr-doped ZnO microrod array samples.

Figure 2. SEM images of (a) undoped, (b) 1.07 % Cr-, (c) 2.49 % Cr and (d) 4.63 % Cr-doped ZnO microrod array samples.

Figure 3. XPS survey spectra of undoped and 4.63 % Cr-doped ZnO microrod array showing binding energy spectrum of Cr 2 p and Gaussian fitting in inset

Figure 4. Optical transmission spectra of undoped, 1.07 % Cr-, 2.49 % Cr and 4.63 % Cr-doped ZnO microrod array samples

Figure 5. Plots of $(\alpha h\upsilon)^2$ versus $(h\upsilon)$ for undoped, 1.07 % Cr-, 2.49 % Cr and 4.63 % Cr-doped ZnO microrod array samples.

Figure 6. PL spectra of undoped, 1.07 % Cr-, 2.49 % Cr and 4.63 % Cr-doped ZnO microrod array samples recorded at 10 K. The intensities of the samples are normalized so that the UV peak at ~ 3.361 eV has the same value for all samples. The actual spectra showed a monotonic reduction in UV peak intensity of about a factor of 6 from the undoped to the 4.63% Cr-doped sample.

Figure 7. Room temperature M-H curves of 1.07 % Cr-, 2.49 % Cr- and 4.63 % Cr-doped ZnO microrod array samples.

Figure 8. Temperature dependence of magnetization of 2.49 % Cr-doped ZnO microrod array sample.

Table Captions

Table 1. Actual atomic concentrations of Zn, O or Cr in undoped and 2 % Cr-, 4 % Cr- and 6 % Cr-doped ZnO microrod array samples

Table 2. Binding energies of Zn and Cr in undoped and 4.63 % Cr-doped ZnO microrod array samples.

Table 1

Sample	**at %**		
	Cr	Zn	O
ZnO	-	49.02	50.98
2 % Cr doped ZnO	1.07	42.64	56.29
4 % Cr doped ZnO	2.49	40.19	57.32
6 % Cr doped ZnO	4.63	38.93	56.45

Table 2

Sample	**Zn $2p_{3/2}$ (eV)**	**Zn $2p_{1/2}$ (eV)**	**Cr $2p_{3/2}$ (eV)**	**Cr $2p_{1/2}$ (eV)**
ZnO	1022.00	1045.28	-	-
4.63 % Cr-doped ZnO	1021.88	1044.98	577.34	586.22

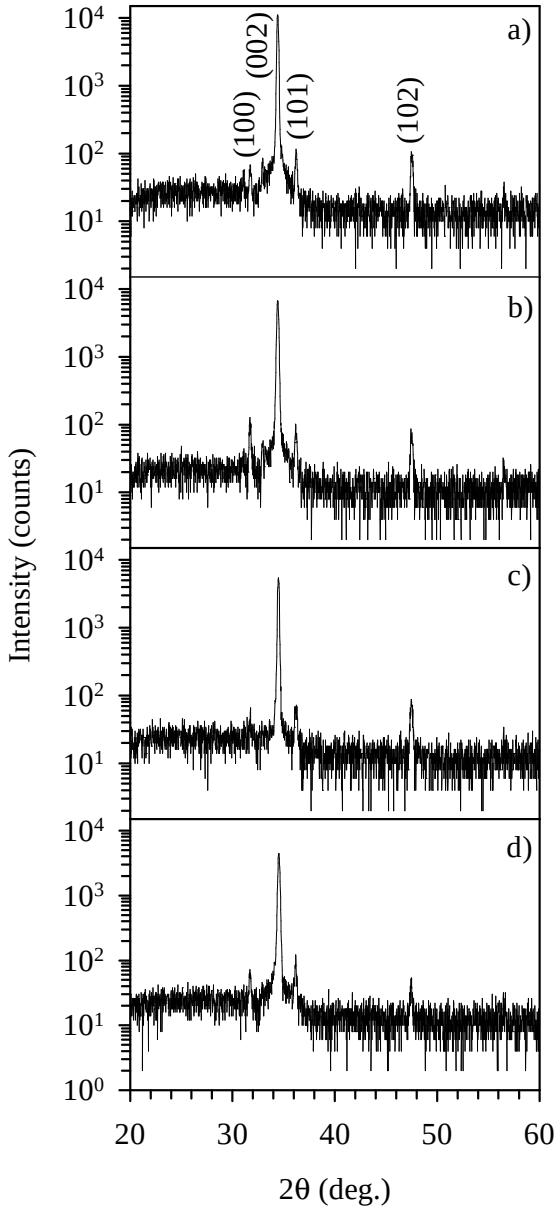
a)
b)
c)
d)
(100)
(002)
(101)
(102)
Intensity (counts)
2θ (deg.)
10^0
10^1
10^2
10^3
10^4
20
30
40
50
60

Figure 1

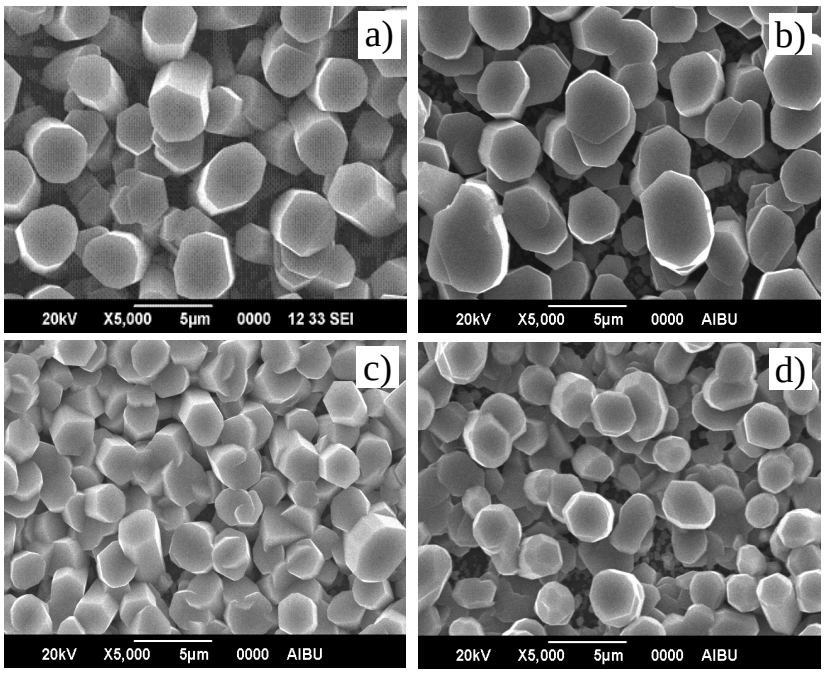
a)
20kV X5,000 5µm 0000 12 33 SEI
b)
20kV X5,000 5µm 0000 AIBU
c)
20kV X5,000 5µm 0000 AIBU
d)
20kV X5,000 5µm 0000 AIBU

Figure 2

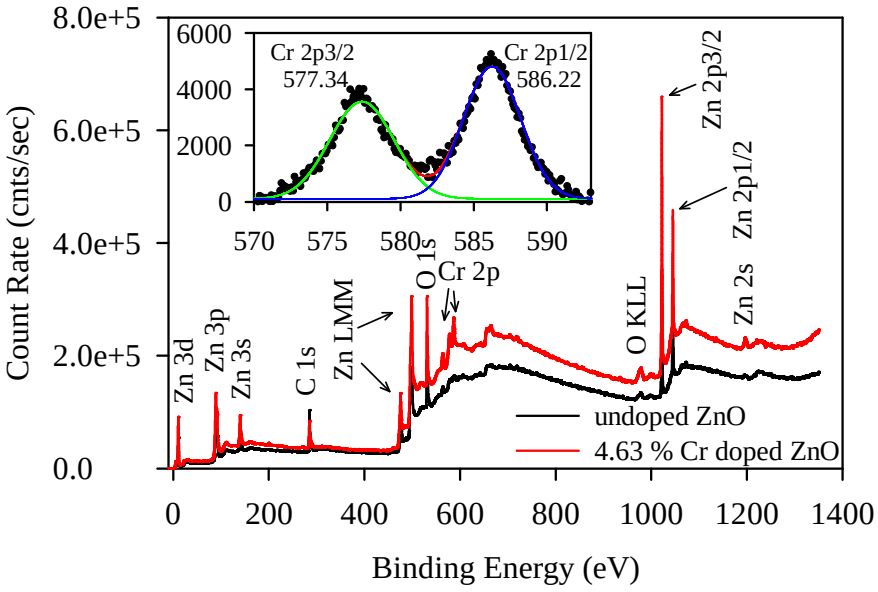

Figure 3

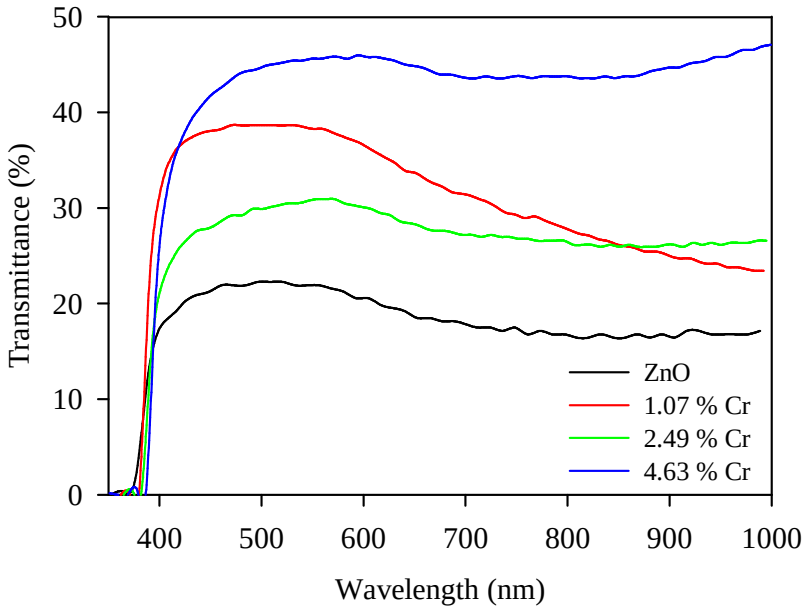

Figure 4

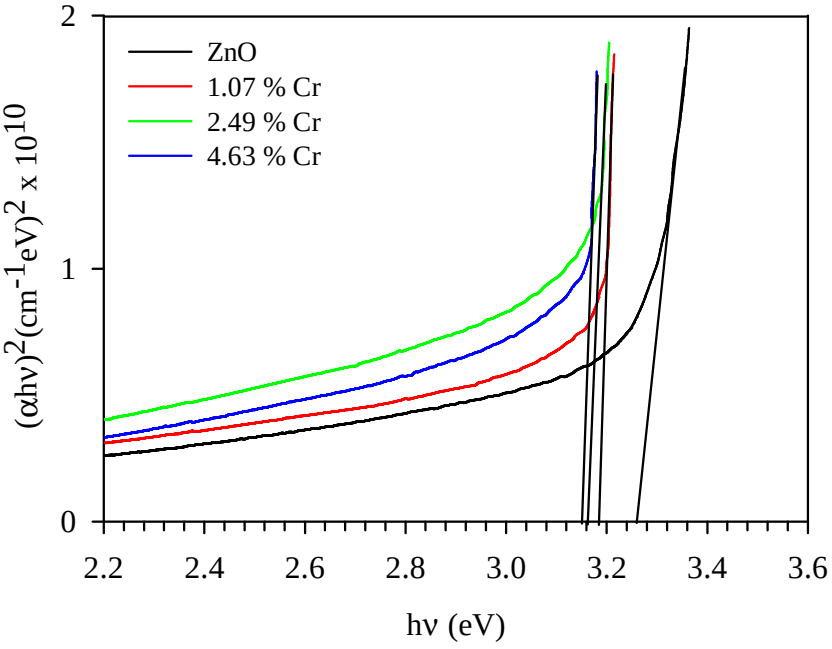

Figure 5

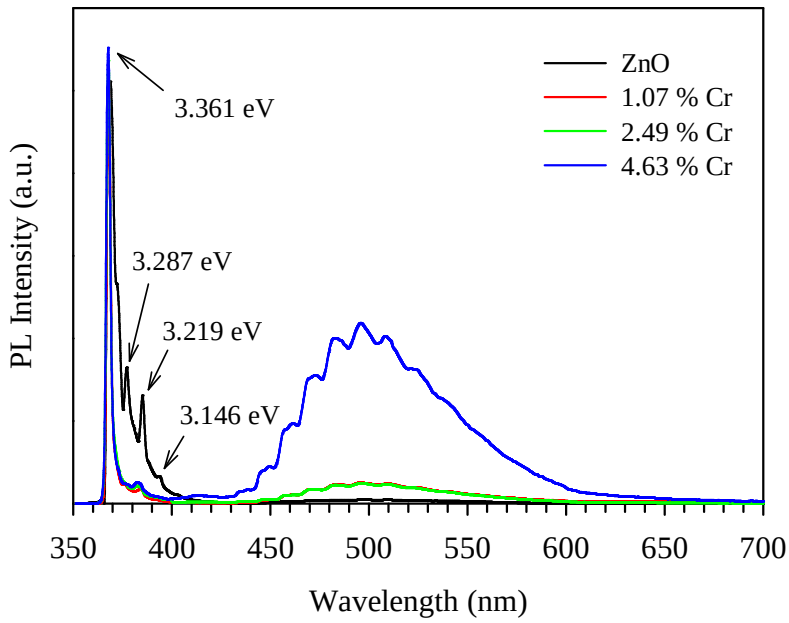

Figure 6

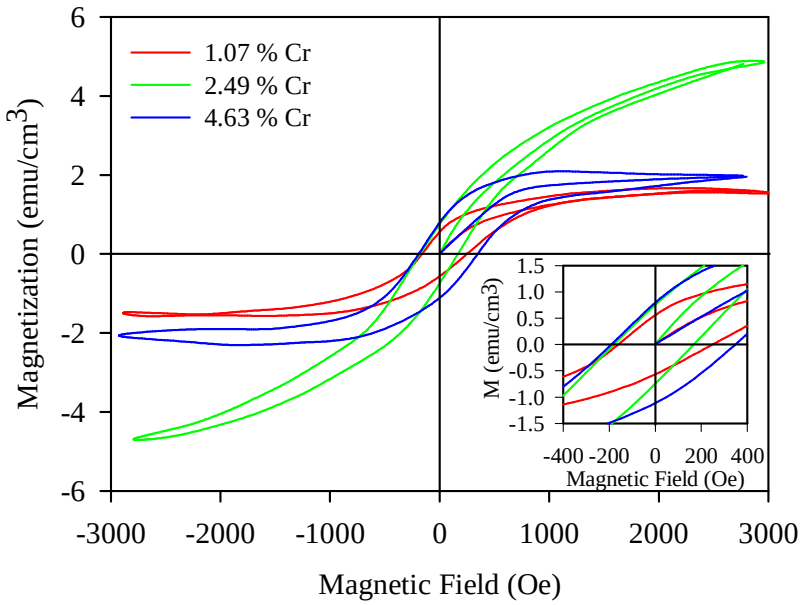

Figure 7

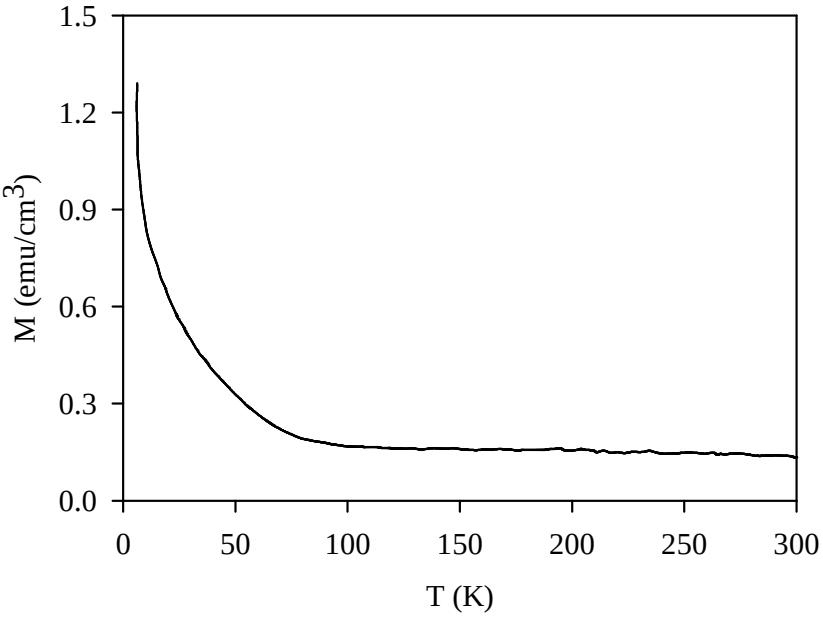

Figure 8

References

[1] Tanaka M and Higo Y 2001 *Phys. Rev. Lett.* **87** 26602

[2] Pearton S J, Abernathy C R, Overberg M E, Thaler G T, Norton D P, Theodoropoulou N, Hebard A F, Park Y D, Ren F, Kim J and Boatner L A 2003 *J. Appl. Phys.* **93** 1

[3] Wang Y X, Liu H, Li Z Q, Zhang X X, Zheng R K and Ringer S P 2006 *Appl. Phys. Lett.* **89** 042511

[4] Xu W Z, Ye Z Z, Zeng Y J, Zhu L P, Zhao B H, Jiang L, Lu J G, He H P and Zhang S B 2006 *Appl. Phys. Lett.* **88** 173506

[5] Tu Z C and Hu X 2006 *Phys. Rev. B* **74** 035434

[6] Mitra P, Chatterjee A P and Maiti H S 1998 *Mater. Lett.* **35** 3

[7] Ueda K, Tabata H and Kawai T 2001 *Appl. Phys. Lett.* **79** 988

[8] Sharma P, Gupta A, Rao K V, Owens F J, Sharma R, Ahuja R, Guillen J M O, Johansson B and Gehring G A 2003 *Nat. Mater.* **2** 673

[9] Liu X X, Lin F T, Sun L L, Cheng W J, Ma X M and Shi W Z 2006 *Appl. Phys. Lett.* **88** 062508

[10] Dietl T, Ohno H, Matsukura F, Cibert J and Ferrand D 2000 *Science* **287** 1019

[11] Sato K and Katayama-Yoshida H 2002 *Semicond. Sci. Tech.* **17** 367

[12] Roberts B K, Pakhomov A B, Shutthanandan V S and Krishnan K M 2005 *J. Appl. Phys.* **97** 10D310

[13] Jin Z, Fukumura T, Kawasaki M, Ando K, Saito H, Sekiguchi T, Yoo Y Z, Murakami M, Matsumoto Y, Hasegawa T and Koinuma H 2001 *Appl. Phys. Lett.* **78** 3824

[14] Lee H J, Jeong S Y, Hwang J Y and Cho C R 2003 *Europhys. Lett.* **64** 797

[15] Philipose U, Nair S V, Simon T, De Souza C F, Aouba S, Hill R H and Ruda H E 2006 *Appl. Phys. Lett.* **88** 263101

[16] Cheng Z X, Wang X L, Dou S X, Ozawa K, Kimura H and Munroe P 2007 *J. Phys. D: Appl. Phys.* **40** 6518

[17] Sato K and Katayama-Yoshida H 2000 *Jpn. J. Appl. Phys. Part 2* **39** L555

[18] Coey J M D, Douvalis A P, Fitzgerald C B and Venkatesan M 2004 *Appl. Phys. Lett.* **84** 1332

[19] Murali K R 2007 *J. Phys. Chem. Solids* **68** 2293

[20] Kumar P M R, Kartha S C, Vijayakumar K P, Singh F and Avasthi D K 2005 *Mater. Sci. Eng. B* **117** 307

[21] Bacaksiz E, Aksu S, Yılmaz S, Parlak M and Altunbaş M 2010 *Thin Solid Films* **518** 4076

[22] Deng H, Russell J J, Lamb R N and Jiang B 2004 *Thin Solid Films* **458** 43

[23] Tusche C, Meyerheim H L and Kirschner J 2007 *Phys. Rev. Lett.* **99** 026102

[24] Kizler P, He J, Clarke D R and Kenway P R 1996 *J. Am. Ceram. Soc.* **79** 3

[25] Morkoç H and Özgür Ü 2009 *Zinc Oxide: Fundamentals, Materials and Device Technology* (Weinheim: Wiley-Vch)

[26] Wang R C and Lin H Y 2011 *Mater. Chem. Phys.* **125** 263

[27] Peter Y Y and Cardona M 2001 *Fundamentals of Semiconductors: Physics and Material Properties* (Berlin: Springer)

[28] Reddy K M, Benson R, Hays J, Thurber A, Engelhard M H, Shutthanandan V, Hanson R, Knowlton W B and Punnoose A 2007 *Sol. Energ. Mat. Sol. C* **91** 1496

[29] Maetaki A. Yamamoto M, Matsumoto H and Kishi K 2000 *Surf. Sci.* **445** 80

[30] Xu C, Hassel M, Kuhlenbeck H and Freund H J 1991 *Surf. Sci.* **258** 23

[31] Yang Y C, Song C, Wang X H, Zeng F and Pan F 2008 *J. Appl. Phys.* **103** 074107

[32] Xu C, Yang K, Liu Y, Huang L, Lee H, Cho J and Wang H 2008 *J. Phys. Chem. C* **112** 19236

[33] Moudler J F, Stickle W F, Sobel P E and Bomben K D 1992 *Handbook of X-ray Photoelectron Spectroscopy* (Minnesota:Perkin-Elmer)

[34] Lee J H, Yeo B W and Park B O 2004 *Thin Solid Films* **457** 333

[35] Hu Y M, Chen Y T, Zhong Z X, Yu C C, Chen G J, Huang P Z, Chou W Y, Chang J and Wang C R 2008 *Appl. Surf. Sci.* **254** 3873

[36] Li L, Wang W, Liu H, Liu X, Song Q and Ren S 2009 *J. Phys. Chem. C* **113** 8460

[37] Meyer B K, Alves H, Hofmann D M, Kriegseis W, Forster D, Bertram F, Christen J, Hoffmann A, Straßburg M, Dworzak M, Haboeck U and Rodina A V 2004 *Phys. Status Solidi b* **241** 231

[38] Elliott R J 1957 *Phys. Rev.* **108** 1384

[39] Liang W Y and Yoffe A D 1968 *Phys. Rev. Lett.* **20** 59

[40] Klingshirn C F 2006 *Semiconductor Optics* (Berlin: Springer)

[41] Reynolds D C, Look D C, Jogai B, Jones R L, Litton C W, Harsch W and Cantwell G 1999 *J. Lumin.* **82** 173

[42] Chen X H, Zhang H T, Wang C H, Luo X G and Li P H 2002 *Appl. Phys. Lett.* **81** 4419

[43] Roberts B K, Pakhomov A B and Krishnan K M 2008 *J. Appl. Phys.* **103** 07D133

[44] Liu H, Zhang X, Li L, Wang Y X, Zheng R K, Ringer S P, Zhang B and Zhang X X 2007 *Appl. Phys. Lett.* **91** 072511

[45] Hong H, Sakai J, Huong N T, Poirot N and Ruyter A 2005 *Phys. Rev. B* **72** 045336

[46] Li Y, Li Y, Zhu M, Yang T, Huang J, Jin H and Hu Y 2010 *Solid State Commun.* **150** 751

[47] Liu Y, Yang J, Guan Q, Yang L, Zhang Y, Wang Y, Feng B, Cao J, Liu X, Yang Y and Wei M 2009 *J. Alloy. Compd.* **486** 835

[48] Chu D, Zeng Y P and Jiang D 2007 *Solid State Commun.* **143** 308

[49] Xing G Z, Yi J B, Tao J G, Liu T, Wong L M, Zhang Z, Li G P, Wang S J, Ding J, Sum T C, Huan C H A and Wu T 2008 *Adv. Mater.* **20** 3521

[50] Xing G Z, Yi J B, Wang D D, Liao L, Yu T, Shen Z X, Huan C H A, Sum T C, Ding J and Wu T 2009 *Phys. Rev. B* **79** 174406

[51] Wang F, Pang Z, Lin L, Fang S, Dai Y and Han S 2010 *Phys. Rev. B* **81** 134407

[52] Kittilstved K R, Schwartz D A, Tuan A C, Heald S M, Chambers S A and Gamelin D R 2006 *Phys. Rev. Lett.* **97** 037203

[53] Satoh I and Kobayashi T 2003 *Appl. Surf. Sci.* **216** 603